Please cite this paper as

Li J and Zhu S (2021) Advanced Vibration Isolation Technique using Versatile Electromagnetic Shunt Damper with Tunable Behavior. Engineering Structures. 242: 112053. https://doi.org/10.1016/j.engstruct.2021.112503

Advanced Vibration Isolation Technique using Versatile Electromagnetic Shunt Damper with Tunable Behavior

Jin-Yang LI[1], Songye ZHU[1]*,

[1] Department of Civil and Environmental Engineering, The Hong Kong Polytechnic University, Hung Hom, Kowloon, Hong Kong, China

* Corresponding author: Dr Songye Zhu, Email: songye.zhu@polyu.edu.hk

Abstract:

Electromagnetic shunt damper (EMSD) is an emerging damper type capable of mimicking conventional mechanical dampers using their electrical circuit counterparts. Damping, stiffness, and inertance within mechanical domain can be emulated by resistance, inductance, and capacitance from electrical domain, respectively. In particular, four representative conventional damper types, namely, viscous fluid damper (VFD), viscoelastic damper (VED), inerter damper (ID), and tuned inerter damper (TID), are emulated by an EMSD in this paper, thereby forming EMSD-VFD, EMSD-VED, EMSD-ID and EMSD-TID, respectively. Their control performances when installed in a vibration isolation system are subsequently studied both analytically and experimentally. The behavior of EMSD can be easily tuned by changing the external circuits connected to the electromagnetic damper. Moreover, these four types of EMSDs possess complementary isolation performances across the frequency spectrum, which implies that different optimal circuits should be selected in different frequency bands to achieve the best isolation performance. A broadband vibration isolation technique by automatically switching among sub-circuits integrated in a single circuit board, which has not been realized in the current study, will be a promising future research direction.

Keywords: electromagnetic shunt damper, isolation, inerter damper, tuned inerter damper, tunable

List of Nomenclature

Symbol	*Description*	*Symbol*	*Description*
c_d	Equivalent damping coefficient emulated by EMSD	L_0	Motor inner inductance
c_h	Damping coefficient of the host structure	L_{opt}	optimal inductance
C	Capacitance	m_d	Equivalent inertance emulated by EMSD
C_{opt}	optimal capacitance	M_h	Mass of the host structure
c_p	Parasitic damping coefficient	OP-AMP	Operational amplifier
c_t	total damping coefficient	r	Frequency ratio
c_v	viscous damping from the	R_0	Motor inner resistance
DAQ	Data acquisition	R_1	Resistor 1 in VNIC module

DC	Direct current	R_2	Resistor 2 in VNIC module
EM	Electromagnetic	R_3	Variable resistor 3 (Rheostat) in VNIC module
emf	electromotive force	R_{opt}	Optimal resistance
EMSD	Electromagnetic Shunt Damper	R_t	Total circuit resistance
EMSD-ID	Inerter Damper emulated by Electromagnetic Shunt Damper	R_{VNIC}	Equivalent resistance by VNIC
EMSD-TID	Tuned Inerter Damper emulated by Electromagnetic Shunt Damper	s	Laplace variable
EMSD-VED	Viscoelastic Damper emulated by Electromagnetic Shunt Damper	$S_{1,2}$	Power supply in VNIC module
EMSD-VFD	Viscous Fluid Damper emulated by Electromagnetic Shunt Damper	SDOF	Single Degree of Freedom
F_k	Friction coefficient	TID	Tuned inerter damper
f_v	vibration frequency	VED	Viscoelastic damper
H	transmissibility value (X/Y)	VFD	Viscous Fluid Damper
ID	Inerter damper	VNIC	Negative Impedance Converter with Voltage Inversion
j	Imaginary unit	X	Mass displacement after Laplace transformation
k_2	Damping coefficient	Y	Ground displacement after Laplace transformation
k_d	Equivalent stiffness emulated by EMSD	ζ	damping ratio
K_{em}	Motor constant	λ	Stiffness ratio
K_h	Spring stiffness of the host structure	μ	mass ratio
L	Inductance	ω_n	Natural frequency (rad)

1. Introduction

Excessive ground vibrations may adversely affect the safety and functionality of civil and mechanical structures, as well as the comfort level of occupants. Common ground vibration sources include, but are not limited to, earthquake, construction, traffic and machinery induced vibrations. In this regard, various vibration isolation techniques have been implemented to mitigate the negative impact associated with the ground-induced vibrations. Vibration isolation systems are commonly categorized into active, semi-active and passive types, which correspond to the use of passive, semi-active and active dampers or devices. Soong [1] provided a detailed review of active isolation techniques in civil engineering. Datta [2] later updated the review and extend the scope to cover some semi-active control techniques for seismic isolations. Karnopp [3] carried out a brief review on active and semi-active vibration suspension techniques in platforms and vehicles. Symans and Constantinou [4] gave a review on semi-active control systems for seismic protection. Jalili [5] conducted a comparative study and analysis of semi-active vibration control on vehicles suspensions. Buckle [6] and Parulekar and Reddy [7] reviewed passive control design of structures for seismic response reduction. Housner *et al* [8] gave a thorough review on structural control techniques covering all three types.

Among the aforementioned three types, the isolation techniques using passive dampers have seen the widest applications owing to their inherent control stability and zero power consumption. A variety of passive mechanical dampers, including viscous fluid damper (VFD), viscoelastic damper (VED), inerter damper (ID) and tuned inerter damper (TID), have been investigated in passive isolation systems. Recently, an emerging damper type – electromagnetic shunt damper (EMSD) – has drawn research attention due to its potential to emulate conventional mechanical passive dampers using their electrical counterparts based on the analogue relations between the mechanical and electric systems. Actually, the first reveal of the analogy between the two systems dated back to year 1933 by Firestone [9], in which the capacitance was linked to mass. Until recently, Smith [10] pointed out that a more accurate analogue of capacitance shall be inertance, considering both are two-node elements whereas mass is a typical one-node element. So far, the mechanical elements comprising of damping, stiffness, and inertance can be emulated by their electrical counterparts – resistance, inductance, and capacitance, which lays the foundation of mimicking conventional mechanical dampers using EMSD. Besides, some of the major merits of EMSD over conventional passive dampers are:

a. Compared with mechanical elements, their electrical counterparts are generally more compact in size by orders of magnitude; and this enables the integration of versatile circuit designs into a single board to realize advanced damper behaviors that can barely be achieved by conventional mechanical dampers.

b. Electrical elements are generally cheap owning to the mass production. In addition, unlike mechanical dampers of which the mechanical elements (e.g., spring or damper) are normally specially designed and tailor made, there is no specific end-use requirements on the electrical elements adopted in EMSD as long as they fit the purpose. Thus, abundant options are market available to choose from.

c. The maintenance cost of EMSD is low, given the electric elements can be replaced in the shunt circuit only without interfering the whole damper. For instance, the electromagnetic (EM) transduce do not need to be detached from the primary structure to have the electrical elements replaced. Meanwhile, EMSD can be updated anytime by adjusting its shunt circuit only, that is barely applicable to mechanical dampers.

d. In conventional viscous fluid dampers (VFDs) or magnetorheological dampers (MRDs), local over-heating problem remains a challenge, which will accelerate rubber seal aging and consequently lead to oil leakage problem [11]. In contrast, unwanted kinetic energy will be transformed into electricity in EMSD and then shunted out to its external circuit. Thus, the over-heating of the damper is no longer a concern.

e. Given EMSD converts kinetic energy into electrical energy instead of heat dissipation, potential energy harvesting capability [12-14] is available.

Given the above unique advantages of EMSD, a group of researchers have investigated its applications in base isolation problem. Karnopp [15] discussed the feasibility of implementing EMSD in vehicle suspensions as variable mechanical dampers. Graves *et al* [16] adopted a similar idea by further proposing paralleled resistance to reduce large existing resistance to small one to enhance energy outflow to the external circuit for better isolation performance. Gonzalez-Buelga *et al* [17] coupled an energy harvesting module that is equivalent to a variable resistance (R) or damping coefficient with a TMD in realization of simultaneous base isolation and vibration control performance. Likewise, Ding *et al* [18] showed the energy regeneration circuit of EMSD is equivalent to a pure damping (or equivalent R) and was subsequently applied to the vehicle suspension design. Marneffe *et al* [19] used the series RL circuit to emulate a relaxation isolator and achieved enhanced vibration isolation performance. Yan *et al* [20] introduced negative resistance to the EMSD isolation system and achieved enhanced vibration isolation through RL circuit with enlarged equivalent damping coefficient and auxiliary stiffness. Sasaki *et al* [21] adopted a series RLC resonant shunt circuit to suppress the vibration amplitude of a superconducting levitated body. Liu *et al* [22] coupled EMSD with TMD and subsequently derived optimal series RLC parameters under both forced and ground excitations under H_2 control algorithm. Nakamura *et al* [23] used EMSD and flywheel to provide damping and inertance, respectively. Feasibility of the device was subsequently verified through the control of a framework subjected to seismic input. Later, Gonzalez-Buelga *et al* [24] studied base isolation performance of a single degree-of-freedom (SDOF) system using EMSD (paralleled R and L in series connection to C) in emulation of tuned inerter damper (TID). The authors concluded that such topology provides better control performance than series RLC circuit. Pei *et al* [25] discovered base isolation performance of two multi-resonance circuits configurations (i.e., multi-parallel and multi-series) with both vibration control and energy harvesting abilities under the H_2 optimization of the relative displacement. In particular, the multi-parallel circuit is a paralleled series RLC circuits, and the multi-series circuit is an RLC circuit in series with a paralleled L and series RC. It is claimed better damping performances can be achieved by the multi-mode circuits than the traditional single mode with enhanced broadband control.

However, some deficiencies have also been identified in the existing studies. First, although all the above examples belong the EMSD category, they exhibit different control mechanisms and effects, and should be more accurately distinguished. Second, the existence of the inner resistance of the EM device may considerably jeopardize their control performance. Very recently, Li and Zhu [26] demonstrated successful realization of versatile mechanical damper behaviors, including VFD, VED, ID and TID, using a single EMSD with the facilitation of negative impedance converter with voltage inversion (VNIC). By connecting a single EM transducer to the corresponding shunt circuits, the EMSD can function as EMSD-VFD, EMSD-VED, EMSD-ID, and EMSD-TID. In addition, the feasibility of EMSDs to large-scale applications was validated [27]; and superior vibration mitigation performance has been achieved experimentally by an EMSD-ID to the control a 135m full-scale cable [28].

Inspired by the compact sizes of electrical elements allowing for potential complex circuit design (i.e., advantage point (a)), as well as the unique isolation performances of various EMSDs from previous literatures, an EMSD-VNIC-based isolator with tunable behaviors is proposed in this paper and subsequently studied. Herein, the tunable behaviors are achieved by the combination of various sub-circuits, each of which emulates a typical passive damper type, and the flexible switch among these sub-circuits. In this paper, the four EMSD isolator types (i.e., EMSD-VFD, EMSD-VED, EMSD-ID, and EMSD-TID) are analyzed quantitively first to suggest their individual characteristics observed in transmissibility functions. Next, experimental verification is carried out to validate the isolation performances of each type to reassure that the discovered characteristic can be physically achieved. By accurately categorizing the EMSD isolator into four types, the following new insights can be obtained in this study: (1) their base isolation mechanisms and performances can be accurately differentiated; (2) the analogy to the mechanical dampers (such as VFD, VED, ID, and TID) can facilitate the understanding of the EMSD isolation performance, as well as their comparison with the traditional passive isolators with these mechanical dampers; and (3) the direct performance comparison of the transmissibility functions not only enables to identify the locally optimal cases among different EMSD types, but also projects another intelligent strategy to switch among various sub-circuits with the lowest transmissibility profile in different frequency bands. Consequently, an advanced vibration isolation strategy using tunable EMSD will be able to be achieved with a broadband isolation performance in the future.

2. EMSD with VNIC

An EMSD refers to an EM transducer (i.e., EM motor) connected to an external shunt circuit, the configuration of which determines the damper behaviors. Given a representative linear EM transducer (e.g., a linear non-commutated direct current (DC) EM motor as adopted in this paper), the relative motion between its two nodes generates back electromotive force (*emf*) at two ends of the coil; and the current passing through the motor coil produces a reactive EM force as

$$\begin{cases} u = K_{\mathrm{em}}(\dot{x} - \dot{y}) \\ f = K_{\mathrm{em}} i \end{cases}, \qquad (1)$$

where u is the *emf* (i.e., open circuit voltage) generated in the EM transducer; $\dot{x} - \dot{y}$ stands for the relative velocity between its two nodes; i is the motor current; f is the EM force induced by the current; and K_{em} is the motor constant determined solely by the physical parameters of the EM motor itself, and is independent from connected shunt circuit (i.e., K_{em} is fixed once EM transducer was manufactured).

Consequently, the fundamental of EMSD is to manipulate the force-velocity relationship of the EM device via an external shunt circuit that regulates the current-voltage relationship. The above electro-mechanical coupling effect of the EM device offers an appealing one-to-one analogue relations between mechanical elements and their electrical counterparts ([28]) as

$$\begin{cases} m_{\mathrm{d}} = K_{\mathrm{em}}^{2} C \\ c_{\mathrm{d}} = K_{\mathrm{em}}^{2} / R \\ k_{\mathrm{d}} = K_{\mathrm{em}}^{2} / L \end{cases}, \tag{2}$$

where R, L and C stand for the resistance, inductance, and capacitance from the electrical domain, respectively; m_{d}, c_{d} and k_{d} are their equivalent mechanical counterparts emulated by EMSD – inertance, damping, and stiffness, respectively.

Eq. (2) serves as the foundation for EMSD to emulate any desired mechanical components using their electrical counterparts. Consequently, Table I provides the mechanical topologies of the selected four damper types (i.e., VFD, VED, ID, and TID) along with their corresponding electrical circuits that enable the EMSD to provide comparable damper behaviors. Nonetheless, due to the existence of inherent resistance (R_0) arising from the coil materials in the motor and other electrical elements (e.g. inductor and connections wires), the actual damper performances of the EMSD will deviate from those of ideal analogies. Thus, Table I includes two parts, namely, ideal and actual analogies that are differentiated by the influence of the inherent resistances. Compared with the idea analogy, the actual analogy scenarios demonstrate the existence of the series connected R_0 and R. Herein, R_0 refers to the inner resistance of EM motor that cannot be removed; and R stands for the overall resistance arising from the external circuit, which may include (1) adjustable resistance (i.e., rheostat), (2) inductor inner resistance, (3) equivalent "negative resistance" granted by the VNIC etc., whichever apply. To avoid complication and highlight the key effects of the inductor and capacitor element in the topologies of EMSD-VED and EMSD-ID, respectively, no parallel R is adopted in the actual circuits, although it is seen in the ideal analogy cases. Thus, the actual EMSD-VED and EMSD-ID cannot perfectly mimic the ideal VED and ID due to the existence of R_0, although they produce very similar mechanical behaviours. The transfer functions in Table I reveals the adverse impact of a large series resistance R_0 that may camouflage the effects of inductance and capacitance in EMSD.

This also highlights the important role of VNIC in all four cases. VNIC provides an equivalent "negative resistance" (i.e., R can take a negative value when VNIC is connected) that can partially cancel the adverse impact of R_0. Consequently, VNIC enlarges the adjustable resistance range. System topology of VNIC module is shown in Fig. 1 as Module B. The other two modules (Module A and Module C) in Fig. 1, represent an EM transducer, and a tunable shunt circuit with four sub-circuits, respectively.

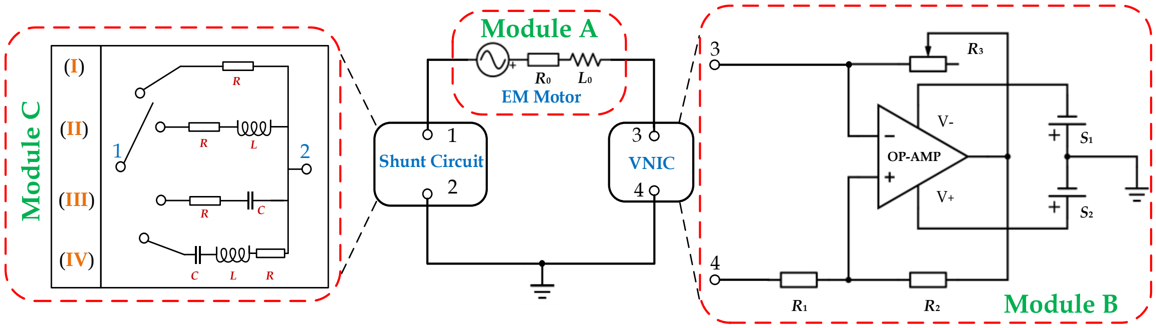

Fig. 1 EMSD with VNIC system (Circuits I-IV coincide with four cases shown in Table I)

In specific, Module A represents an EM transducer that can be equivalently treated as a series connection of an ideal *emf* source, a motor inherent resistance (R_0) and a motor inductance (L_0). Given the low vibration frequency range covered in this paper, the inherent inductance (L_0) can be generally ignored. Module B includes the VNIC circuit comprising one power operational amplifier (OP-AMP), three resistors (i.e., $R_1 - R_3$), and two power sources (i.e., S_1, S_2) supplying the OP-AMP. The equivalent negative resistance (R_{VNIC}) generated by VNIC circuit is

$$R_{\mathrm{VNIC}} = -\frac{R_1 R_3}{R_2}, \tag{3}$$

where R_1 and R_2 function as the voltage divider. Large resistances R_1 and R_2 (e.g., 1 MΩ each) are often taken to minimize power consumption. If we choose $R_1 = R_2$, the equivalent resistance (R_{VNIC}) becomes

$$R_{\mathrm{VNIC}} = -R_3, \tag{4}$$

This equivalent negative resistance can partially offset (i.e., equivalently “cancel”) the inherent resistance, and minimize the total circuit resistance to $R_t = R_0 + R = R_0 - |R_{\mathrm{VNIC}}|$. If R_0 is fully cancelled, the EMSD can theoretically achieve the ideal analogy in Table I. However, this can hardly be achieved due to the power issues in VNIC. More detailed analysis regarding the working mechanism and power issues of VNIC can be found in [28].

Module C of Fig. 1 shows the tunable circuit containing four sub-circuits capable of mimicking the behaviors of the four representative damper types (i.e., VFD, VED, ID, and TID from top to bottom), which are termed EMSD-VFD, EMSD-VED, EMSD-ID, and EMSD-TID in this paper to match those from Table I.

The series combination of Modules A to C depicts the proposed EMSD system with tunable behaviors. Since the series R seen in the branch may be either positive or negative, the total circuit resistance R_t can be either larger or smaller than R_0 in the application.

Table I Analogies between the mechanical and electrical systems of the four representative types

Case #	Mechanical Dampers*	Electromagnetic Shunt Dampers (EMSDs)	$\mathrm{TF}_{\mathrm{EMSD}} = \dfrac{F}{(X-Y)}$	
		IDEAL ANALOGY		
I	VFD 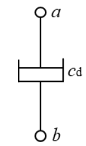	EMSD-VFD 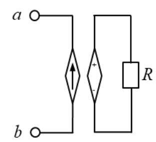	$\dfrac{K_{\mathrm{em}}^2 s}{R}$	(5)
II	VED 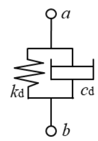	EMSD-VED 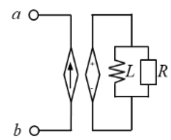	$\dfrac{K_{\mathrm{em}}^2 (Ls+R)}{RL}$	(6)
III	ID 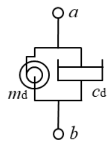	EMSD-ID 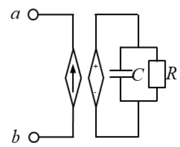	$\dfrac{K_{\mathrm{em}}^2 (RCs^2+s)}{R}$	(7)
IV	TID (series) 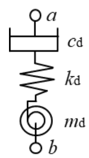	EMSD-TID 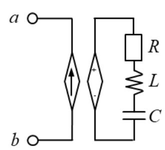	$\dfrac{K_{\mathrm{em}}^2 s}{Ls+R+\dfrac{1}{Cs}}$	(8)
		ACTUAL ANALOGY		
I	VFD 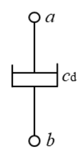	EMSD-VFD 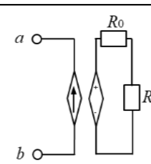	$\dfrac{K_{\mathrm{em}}^2 s}{R+R_0}$	(9)
II	VED 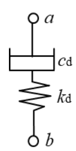	EMSD-VED 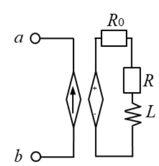	$\dfrac{K_{\mathrm{em}}^2 s}{Ls+(R+R_0)}$	(10)
III	ID 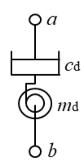	EMSD-ID 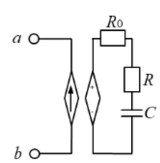	$\dfrac{K_{\mathrm{em}}^2 s}{(R+R_0)+\dfrac{1}{Cs}}$	(11)
IV	TID (series) 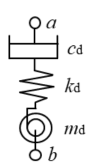	EMSD-TID 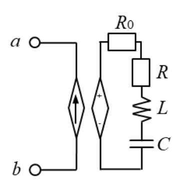	$\dfrac{K_{\mathrm{em}}^2 s}{Ls+(R+R_0)+\dfrac{1}{Cs}}$	(12)

* m_d, k_d, and c_d represent the inertance, stiffness, and damping coefficients of conventional mechanical dampers, respectively.

3. Vibration Isolation with EMSD

3.1. System Description and Analytical Solution

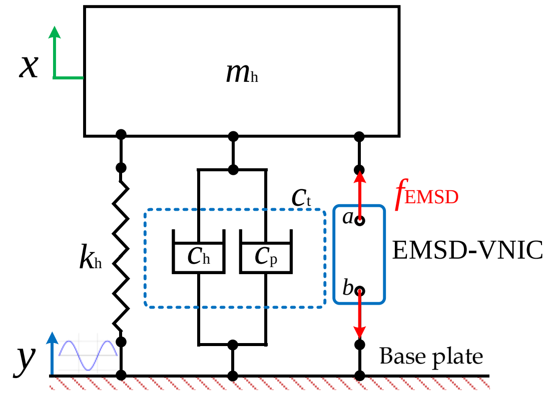

Fig. 2 Schematic of SDOF system under seismic excitation

Fig. 2 shows the schematic of an SDOF system installed with EMSD subjected to ground excitation, where m_h, c_h, and k_h denote the mass, damping and stiffness coefficients of the SDOF host structure, respectively. x and y denote the displacements of the sprung mass and ground motion, respectively. Parasitic damping (c_p) accounting for various mechanical losses of the EMSD (e.g., friction loss, windage loss, magnetic loss etc.) is also taken into consideration. Despite its complex nature, parasitic damping can be estimated on the basis of an equivalent energy approach [29] in form of

$$c_{\mathrm{p}} = \frac{2F_{\mathrm{k}}}{\pi^2 f_{\mathrm{v}} d} + c_{\mathrm{v}} \ , \tag{13}$$

where F_k is the kinetic friction force, c_v is the viscous damping coefficient, f_v is the vibration frequency, and d is the moving amplitude of the EM damper. Essentially, the parasitic damping (c_p) of EMSD and the structural inherent damping (c_h) of EMSD can be treated in parallel connection with other, and can be represented using a total damping coefficient (i.e., $c_{\mathrm{t}} = c_{\mathrm{h}} + c_{\mathrm{p}}$) for easier handling. The two nodes "*a*" and "*b*" in Fig. 2 correspond to those of EMSDs in Table I.

The equation of motion of the isolated SDOF system coupled with EMSD can be written as

$$m_{\mathrm{h}}\ddot{x} + c_{\mathrm{t}}(\dot{x} - \dot{y}) + k_{\mathrm{h}}(x - y) = f_{\mathrm{EMSD}} \ , \tag{14}$$

where the force f_{EMSD} is defined positive when pointing upward on the sprung mass.

Consequently, the transmissibility function (H) can be obtained in the *Laplace* domain as

$$\mathrm{H}(s) = \frac{\mathrm{X}}{\mathrm{Y}} = \frac{(c_{\mathrm{t}}s + k_{\mathrm{h}}) + \mathrm{TF}_{\mathrm{EMSD}}}{(m_{\mathrm{h}}s^2 + c_{\mathrm{t}}s + k_{\mathrm{h}}) + \mathrm{TF}_{\mathrm{EMSD}}} \ , \tag{15}$$

where X and Y correspond to x and y after *Laplace* transformation, respectively. TF_{EMSD} stands for the transmissibility function of the damper force over relative displacement as provided in Table I. As a results, the analytical transmissibility functions of the vibration isolator with different shunt circuits (i.e., corresponding to EMSD-VFD, EMSD-VED, EMSD-ID, and EMSD-TID) can be obtained by substituting the corresponding TF_{EMSD} to Eq. (15).

3.2. Isolation with EMSD-VFD

EMSD-VFD is realized by connecting an EM motor to a pure resistance (*R*) as seen in Table I. With reference to Eq. (9), EMSD-VFD provides an equivalent pure damping of $K_{\mathrm{em}}^2/(R+R_0)$. In particular, the introduction of VNIC to EMSD-VFD expands the achievable damping range, which is originally constrained at R_0, by bringing potential "negative resistance" effect (i.e., $R=-|R_{\mathrm{VNIC}}|$). As a result, $R+R_0$ in Eq. (9) can theoretically equal to any value from infinity to zero, corresponding to a damping value from zero to infinite. Substituting Eq. (9) into (15) derives the transmissibility function of the SDOF system with EMSD-VFD as

$$\mathrm{H}_{\text{EMSD-VFD}}(s)=\frac{\mathrm{X}}{\mathrm{Y}}=\frac{k_{\mathrm{h}}+\left(c_{\mathrm{t}}+K_{\mathrm{em}}^2/R_{\mathrm{t}}\right)s}{(m_{\mathrm{h}}s^2+k_{\mathrm{h}})+\left(c_{\mathrm{t}}+K_{\mathrm{em}}^2/R_{\mathrm{t}}\right)s}\ , \tag{16}$$

where $R_{\mathrm{t}}=R_0+R$ stands for the total circuit resistance. As discussed above, R_{t} can be smaller than R_0 if VNIC is included.

Further substituting $s = \omega j$ into Eq. (16) yields

$$\mathrm{H}_{\text{EMSD-VFD}}(r)=\frac{1+2\left(\zeta_{\mathrm{h}}+\zeta\right)r\cdot j}{(1-r^2)+2\left(\zeta_{\mathrm{h}}+\zeta\right)r\cdot j}, \tag{17}$$

$$\left|\mathrm{H}_{\text{EMSD-VFD}}(r)\right|=\sqrt{\frac{1+4\left(\zeta_{\mathrm{h}}+\zeta\right)^2r^2}{(1-r^2)^2+4\left(\zeta_{\mathrm{h}}+\zeta\right)^2r^2}}\ , \tag{18}$$

where $j=\sqrt{-1}$ is the imaginary unit, $\zeta_{\mathrm{h}}=c_{\mathrm{t}}/\left(2\sqrt{m_{\mathrm{h}}k_{\mathrm{h}}}\right)$ and $\zeta=\left(K_{\mathrm{em}}^2/R_{\mathrm{t}}\right)/\left(2\sqrt{m_{\mathrm{h}}k_{\mathrm{h}}}\right)$ represent the damping ratios contributed by structural inherent damping and EMSD, respectively; $r=\omega/\omega_{\mathrm{n}}$ is the frequency ratio, in which ω is the excitation frequency, and $\omega_{\mathrm{n}}=\sqrt{k_{\mathrm{h}}/m_{\mathrm{h}}}$ is the natural frequency of the SDOF structure. Eqs. (17) and (18) are identical to the classical transmissibility functions of a damped SDOF system, except for the replacement of ζ_{h} by $\zeta_{\mathrm{h}}+\zeta$ reflecting the contribution of an auxiliary equivalent damping of $K_{\mathrm{em}}^2/R_{\mathrm{t}}$ provided by EMSD-VFD.

Two invariant points $\left(r,\left|\mathrm{H}\right|\right)$, namely, $(0,1)$ and $(\sqrt{2},1)$, can be identified regardless of the R_{t} (i.e., ζ) value based on Eq. (18). The amplitude between the two invariant points is always greater than 1, and becomes less than 1 when $r>\sqrt{2}$.

3.3. Isolation with EMSD-VED

EMSD-VED brings equivalent stiffness and damping that are realized by inductance (L) and resistance (R) in the electric circuit, respectively, to the SDOF system. Referring to Table I, the transmissibility function of the SDOF structure installed with EMSD-VED can be obtained by substituting Eq. (10) into Eq. (15) as

$$\mathrm{H}_{\text{EMSD-VED}}(s)=\frac{\mathrm{X}}{\mathrm{Y}}=\frac{c_{\mathrm{t}}s+k_{\mathrm{h}}+K_{\mathrm{em}}^{2}s\big/\left(Ls+R_{\mathrm{t}}\right)}{m_{\mathrm{h}}s^{2}+c_{\mathrm{t}}s+k_{\mathrm{h}}+K_{\mathrm{em}}^{2}s\big/\left(Ls+R_{\mathrm{t}}\right)}, \tag{19}$$

where total resistance R_{t} includes inherent resistances from the EM motor, inductor, connecting wires, and the equivalent "negative resistance" from VNIC.

By further defining stiffness ratio as equivalent stiffness over structural stiffness (i.e., $\lambda=\left(K_{\mathrm{em}}^{2}/L\right)\big/k_{\mathrm{h}}$), Eq. (19) can be rewritten as

$$\left|\mathrm{H}_{\text{EMSD-VED}}(r)\right|=\sqrt{\frac{\left[2\zeta(1+1/\lambda)r^{2}+2\zeta_{\mathrm{h}}r^{2}\right]^{2}+\left(r-4\zeta\zeta_{\mathrm{h}}/\lambda\,r^{3}\right)^{2}}{\left[2\zeta\left((1+1/\lambda)r^{2}-1/\lambda\,r^{4}\right)+2\zeta_{\mathrm{h}}r^{2}\right]^{2}+\left(r\left(1-r^{2}\right)-4\zeta\zeta_{\mathrm{h}}/\lambda\,r^{3}\right)^{2}}}, \tag{20}$$

consisting of the damping ratio, the stiffness ratio, and the frequency ratio.

In particular, if the damping coefficient (c_{t}) of the SDOF structure can be ignored (i.e., $\zeta_{\mathrm{h}}=0$), Eq. (20) can be simplified to

$$\left|\mathrm{H}_{\text{EMSD-VED}}(r)\right|=\sqrt{\frac{4\zeta^{2}(1+1/\lambda)^{2}r^{4}+r^{2}}{4\zeta^{2}\left[(1+1/\lambda)r^{2}-1/\lambda\,r^{4}\right]^{2}+(1-r^{2})^{2}r^{2}}}. \tag{21}$$

3.4. Isolation with EMSD-ID

EMSD-ID employs a capacitor to emulate mechanical inertance. Substituting Eq. (11) into Eq. (15) delivers the transmissibility function of the SDOF system with EMSD-ID as

$$\mathrm{H}_{\text{EMSD-ID}}(s)=\frac{\mathrm{X}}{\mathrm{Y}}=\frac{(c_{\mathrm{t}}s+k_{\mathrm{h}})+K_{\mathrm{em}}^{2}s\Big/\left(R_{\mathrm{t}}+\dfrac{1}{Cs}\right)}{(m_{\mathrm{h}}s^{2}+c_{\mathrm{t}}s+k_{\mathrm{h}})+K_{\mathrm{em}}^{2}s\Big/\left(R_{\mathrm{t}}+\dfrac{1}{Cs}\right)}. \tag{22}$$

Similarly, Eq. (22) can be rewritten as

$$\left|\mathrm{H}_{\text{EMSD-ID}}(r)\right| = \sqrt{\frac{\left[2\zeta(1-\mu r^2)-2\zeta_{\mathrm{h}}\mu r^2\right]^2+\left(\mu r+4\zeta\zeta_{\mathrm{h}}r\right)^2}{\left[2\zeta\left(1-(1+\mu)r^2\right)-2\zeta_{\mathrm{h}}\mu r^2\right]^2+\left(\mu r(1-r^2)+4\zeta\zeta_{\mathrm{h}}r\right)^2}}, \tag{23}$$

where $\mu = \left(K_{\mathrm{em}}^2 C\right)/m_{\mathrm{h}}$ is defined as the mass ratio (i.e., equivalent inertance to structural mass). Herein, the numerator ($K_{\mathrm{em}}^2 C$) represents the emulated inertance that is sometimes referred to rotary mass. Nonetheless, inertance is inherently different from mass given the former is a two-node system linearly dependent to relative acceleration, while the latter responds to its absolute acceleration.

If system damping is negligible (i.e. $\zeta_{\mathrm{h}} = 0$), Eq. (23) can be simplified to

$$\left|\mathrm{H}_{\text{EMSD-ID}}(r)\right| = \sqrt{\frac{4(1-\mu r^2)^2\zeta^2+\mu^2 r^2}{4[1-(1+\mu)r^2]^2\zeta^2+\mu^2(1-r^2)^2 r^2}}, \tag{24}$$

which corresponds to the mechanical topology C2 in reference [30]. As suggested by Hu, Chen, Shu and Huang [30], the introduction of the inertance into the SDOF structure will reduce both the resonant frequency and peak amplitude of the transmissibility curve. In addition, one special feature of ID or EMSD-ID is the bounce-back (or tail-up) effect at high frequencies if the system damping is low. This is different from the curve of EMSD-VFD, in which the tail part is monotonically decreasing at high frequencies.

3.5. Isolation with EMSD-TID

EMSD-TID consists of a mixture of capacitance, resistance, and inductance representing inertance, damping, and stiffness effects, respectively. In fact, any combination of the mentioned three elements can be treated as an EMSD-TID. Due to simultaneous existence of capacitance and inductance (i.e., equivalent inertance and stiffness), almost all EMSD-TID patterns offer an additional DOF above the original SDOF system that leads to a two-peak transmissibility curve. In order to provide a general understanding of the characteristics of EMSD-TID, one typical series-type *RLC* resonant circuit (i.e., Case IV from Table I) is adopted in our study to demonstrate its unique features. Notably, all previous three cases (i.e., Cases I - III) can be regarded as special cases of EMSD-TID (Case IV), given the elements are connected in series (i.e., no parallel resistance is added referring to actual analogy scenario in Table I). Consequently, the transfer function for EMSD-TID can be obtained by substituting Eq. (12) into Eq. (15) as

$$\mathrm{H}_{\text{EMSD-TID}}(s) = \frac{\mathrm{X}}{\mathrm{Y}} = \frac{(c_{\mathrm{t}}s+k_{\mathrm{h}})+K_{\mathrm{em}}^2 s\Big/\left(Ls+R_{\mathrm{t}}+\dfrac{1}{Cs}\right)}{(m_{\mathrm{h}}s^2+c_{\mathrm{t}}s+k_{\mathrm{h}})+K_{\mathrm{em}}^2 s\Big/\left(Ls+R_{\mathrm{t}}+\dfrac{1}{Cs}\right)}. \tag{25}$$

After substituting $s = \omega j$, Eq. (25) can be rewritten as

$$\left|\mathrm{H}_{\text{EMSD-TID}}(r)\right| = \sqrt{\frac{\left[2\zeta\left(1-\mu\left(1+1/\lambda\right)r^2\right)-2\zeta_{\mathrm{h}}\mu r^2\right]^2+\left[\mu r+4\zeta\zeta_{\mathrm{h}}r\left(1-\mu/\lambda\, r^2\right)\right]^2}{\left[2\zeta\left(1-\left(1+\mu+\mu/\lambda\right)r^2+\mu/\lambda\, r^4\right)-2\zeta_{\mathrm{h}}\mu r^2\right]^2+\left[\mu r\left(1-r^2\right)+4\zeta\zeta_{\mathrm{h}}r\left(1-\mu/\lambda\, r^2\right)\right]^2}} \cdot \quad (26)$$

If the system damping (c_{t}) is negligible (i.e., $\zeta_{\mathrm{h}}=0$), Eq. (26) can be further simplified to

$$\left|\mathrm{H}_{\text{EMSD-TID}}(r)\right| = \sqrt{\frac{4\zeta^2(1-\mu(1+1/\lambda)r^2)^2+\mu^2r^2}{4\zeta^2[1-(1+\mu+\mu/\lambda)r^2+\mu/\lambda\, r^4]^2+\mu^2(1-r^2)^2r^2}}\,, \quad (27)$$

which corresponds to the mechanical topology C4 in [30]. As suggested in [30], the optimal frequency ratio and damping ratio can be determined as

$$\lambda_{\mathrm{opt}}=\mu\ , \quad (28)$$

$$\zeta_{\mathrm{opt}}=\sqrt{\frac{\zeta_{\mathrm{p}}^2+\zeta_{\mathrm{q}}^2}{2}}\ , \quad (29)$$

where $$\zeta_{\mathrm{p,q}}^2=\frac{\mu^2\left(1\mp\sqrt{\mu/(\mu+2)}\right)}{4[(1+\mu)\sqrt{\mu/(\mu+2)}\mp\mu][(3+\mu)\sqrt{\mu/(\mu+2)}\pm\mu]}\,, \quad (30)$$

μ is the equivalent mass ratio to be initially assigned by the designer, ζ_{p} and ζ_{q} seen in Eq. (29) stand for the optimal damping ratios enabling local peaks at the two invariant points (p , q) of Eq. (27), respectively. Provided the flat peaks cannot be simultaneously achieved at these two locations, the optimal damping ratio (ζ_{opt}) in Eq. (30) is eventually assigned as the root mean square of ζ_{p} and ζ_{q} (i.e., Eq. (29)).

Consequently, on the basis of the equivalent relationships $\mu=\left(K_{\mathrm{em}}^2C\right)/m_{\mathrm{h}}$, $\lambda=\left(K_{\mathrm{em}}^2/L\right)/k_{\mathrm{h}}$, and $\zeta=\left(K_{\mathrm{em}}^2/R_{\mathrm{t}}\right)/\left(2\sqrt{m_{\mathrm{h}}k_{\mathrm{h}}}\right)$, the optimal parameters for the electric elements are determined as

$$C_{\mathrm{opt}}=\frac{\mu m_{\mathrm{h}}}{K_{\mathrm{em}}^2}\,, \quad (31)$$

$$L_{\mathrm{opt}}=\frac{K_{\mathrm{em}}^2}{\mu k_{\mathrm{h}}}\,, \quad (32)$$

$$R_{\mathrm{opt}}=\frac{K_{\mathrm{em}}^2}{2\zeta_{\mathrm{opt}}\sqrt{m_{\mathrm{h}}k_{\mathrm{h}}}}\,, \quad (33)$$

4. Experimental Setup

Experimental investigations were further conducted to verify the isolation performances of the EMSD-VNIC system in emulation of the aforementioned four types of conventional mechanical dampers. Fig. 3(a) shows a photo of the overall experimental setup established on a shake table. Fig. 3(b) and (c) shows a detailed photo and schematic of the SDOF frame installed with an EM transducer, respectively. The inverted SDOF structure consists of a mass plate hung by four vertical springs to the aluminum frame that is subjected to ground excitations. The design of the inverted SDOF configuration is to prevent the buckling of the springs under compression that may induce excessive nonlinear behaviors.

Fig. 4 shows a flowchart of the experimental setup consisting of three major modules, namely, (a) the loading module (i.e., the shake table), (b) the SDOF structure module equipped with EMSD-VNIC, and (c) the data acquisition (DAQ) module. PC1 in Fig. 3(a) functioned as a signal generator and generated the desired input signals to a signal amplifier. The amplified signals then drove the shake table (part #: APS 420) to produce regulated ground excitations and excite the SDOF structure. The EMSD (i.e., the EM motor connected to shunt circuits) provided damper forces to suppress the vibration of the SDOF structure.

In terms of the EMSD-VNIC module, it essentially consists of an EM motor (part #: Baldor LMNM2-1F5-1F1) connected between the mass plate and shake table, a VNIC module, and an external shunt circuit. Fig. 5(a) shows photo of the VNIC circuit built on a breadboard; and Fig. 5(b) - (d) shows the other electrical components used in the shunt circuit: capacitor, inductor, and rheostat (variable resistor), respectively.

The ground motion incorporates two types: (1) sinusoidal sweeping excitation, and (2) single-frequency sinusoidal excitation. For sinusoidal sweeping input, a slow sweeping rate of 0.1 Hz/s within the range of interest was implemented to ensure a pseudo steady-state response could be achieved at any given frequency (or any time). Single-frequency sinusoidal excitations was later supplied to examine the performance at resonant and high frequencies.

The signals of interest, including motor current, motor voltage, control force, and accelerations of the shake table and mass plate, are measured with corresponding sensors and recorded by a DAQ module (part #: Kyowa EDX-100A). In specific, three accelerometers (part #: B&K 4370) are deployed to the vibration isolation system (i.e., two placed symmetrically on the mass plate and one on the base plate as seen in Fig. 3(c)). The average of the two top accelerations is used as the mass acceleration to avoid the side-effect induced from plate fluttering. Consequently, the transmissibility curve (i.e., X/Y) can be plotted as the ratio of the accelerations of the mass plate and base plate.

Detailed physical parameters of the overall experimental setup can be found in Table II. The physical parameters of the EM motor are determined based on the measurements using an *LCR* meter (part #: Hioki 3522-50). Herein, the effect of motor inner inductance L_0 is negligible within the input frequency range of interest (i.e., ωL_0 can be ignored comparing to R_0 and shunt circuit impedance).

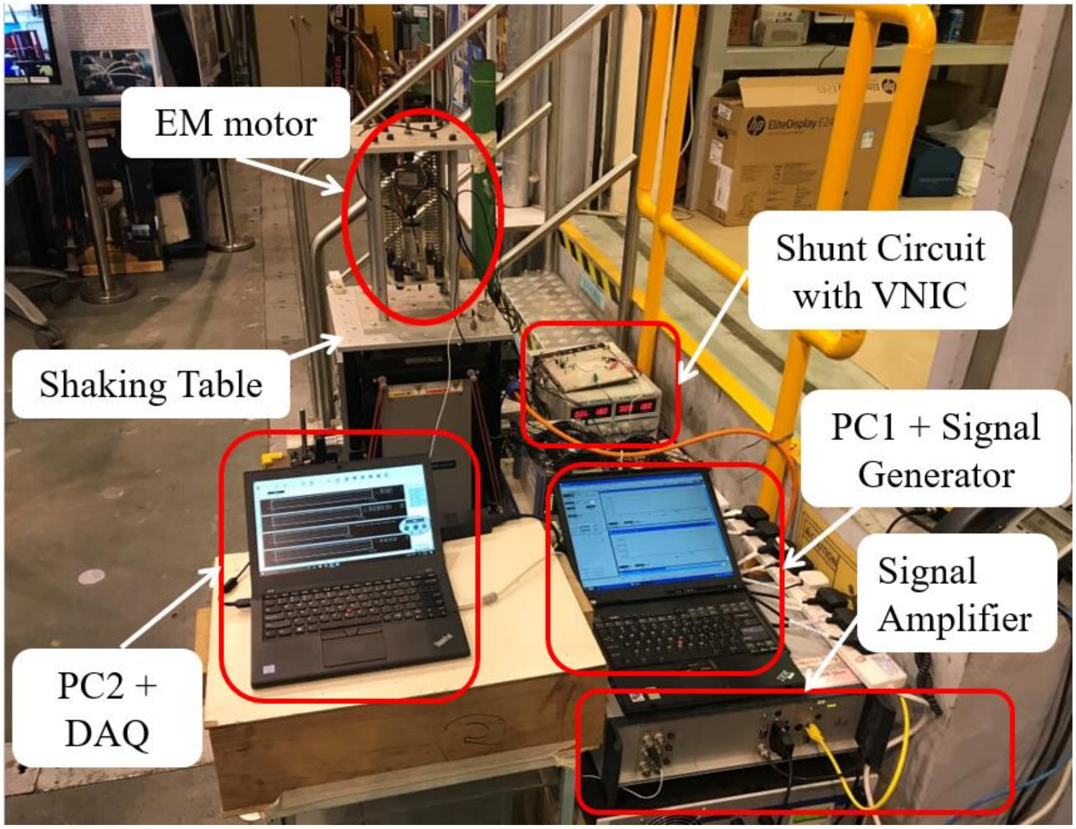

(a) Photo of overall experimental setup

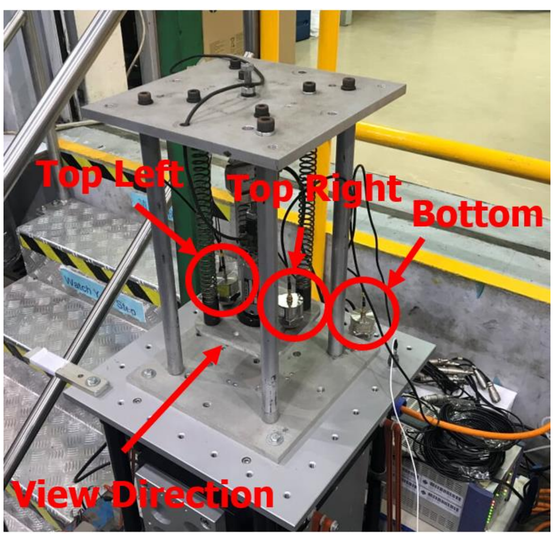

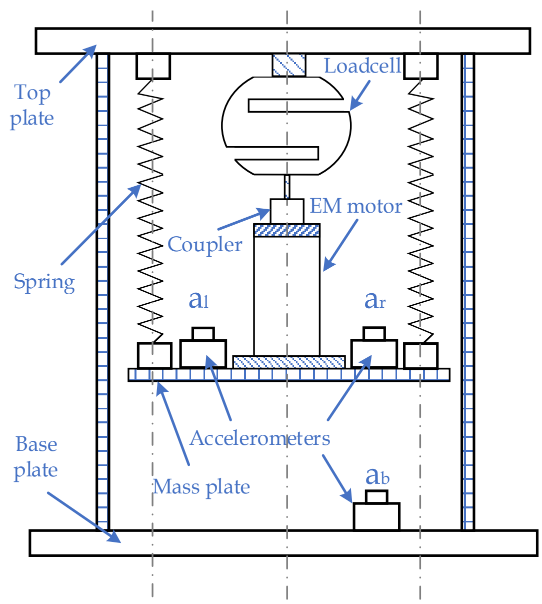

(b) Photo of vibration islation table (c) Schematic of vibration isolation table

Fig. 3 Experimental setup of vibration isolation table with EMSD

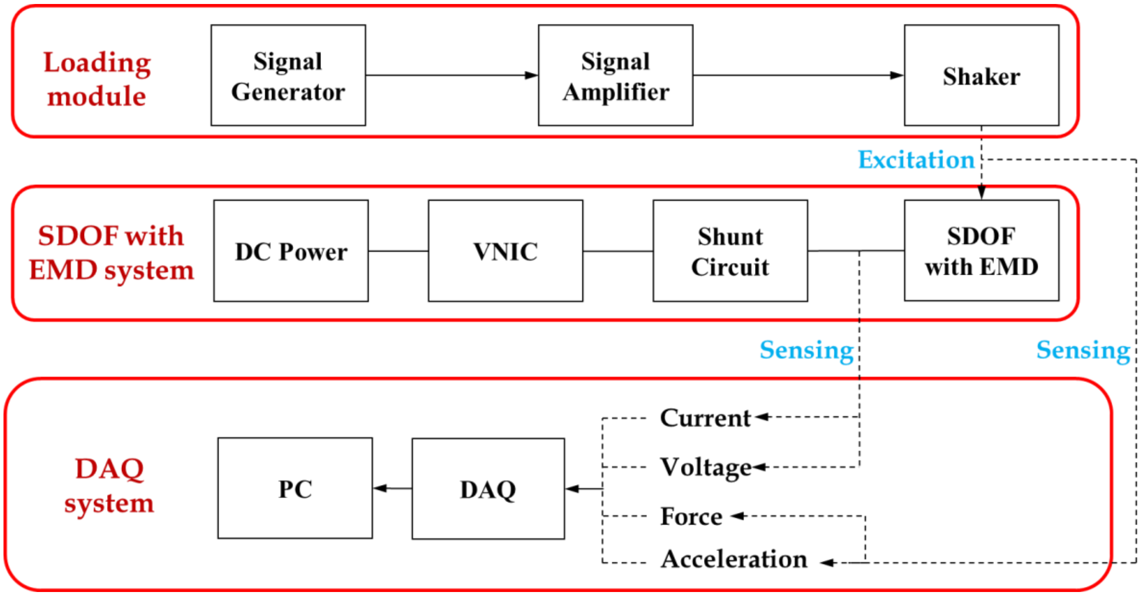

Fig. 4 The flowchart showing the experimental setup of EMSD isolation

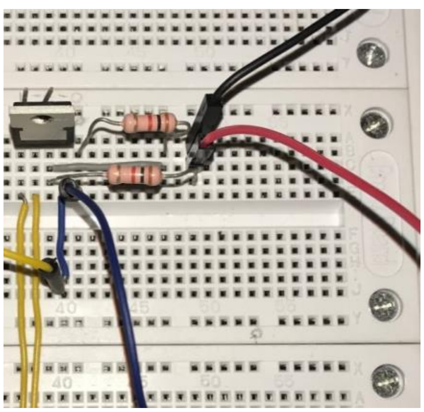

(a) VNIC

(b) Capacitor

(c) Inductor

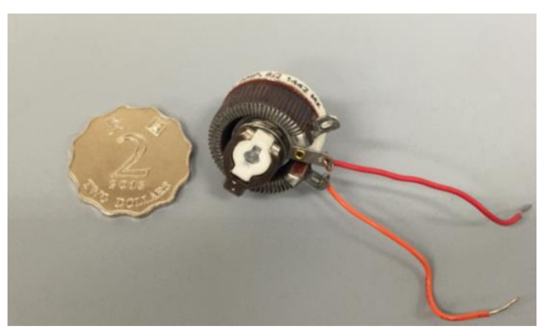

(d) Rheostat (variable resistor)

Fig. 5 Electric elements used in the shunt circuit of EMSD

Table II Major parameters of SDOF & EMSD-VNIC systems

Parameters		Symbol	Value (Unit) / Description
SDOF structure	Plate mass	m_h	2.2 kg
	Spring stiffness	k_h	3000 N/m
	Damping coefficient	c_h	1.24 Ns/m
	Natural frequency	ω_n	36.93 rad/s (5.88Hz)
Motor	Motor constant	K_{em}	7.474 Vs/m (or N/A)
	Motor inner resistance	R_0	3.8 Ω
	Motor inner inductance	L_0	0.003 H
	Friction coefficient	F_k	0.4994 N
	Damping coefficient	c_v	3.126 Ns/m
	Parasitic damping	c_p	8 Ns/m
VNIC	OP-AMP		Type: Apex PA75CD
	Resistor	R_1	1 MΩ
	Resistor	R_2	1 MΩ
	Rheostat	R_3	0~12 Ω

5. Experimental Results and Analysis:

The EMSD connects to four types of shunt circuits to emulate corresponding conventional mechanical dampers. The experimental cases for EMSD-VFD, EMSD-VED, EMSD-ID and EMSD-TID are denoted as Cases I – IV, respectively. Table III summarizes all test scenarios, including shunt circuit parameters and their equivalent mechanical parameters calculated on the basis of Eq. (2). Each case includes different circuits parameters denoted by sub-cases. The parameter selection in these sub-cases aims to reflect the effects of the major control parameters in different types of EMSDs through the comparison. As aforementioned, no paralleled R is included in Case II (EMSD-VED) and Case III (EMSD-ID) for simplicity without losing the core ideas (i.e., equivalent stiffness or inertance effects). Cases in which $R_t < R_0$ indicate the use of VNIC to partially "cancel" the inner resistance R_0. To minimize the adverse impact of inner resistance, R_t is cancelled to be $\leqslant 1$ Ω, which is adequately small in comparison with the overall impedance of the circuit. Extremely small values of R_t are not attempted because of the potential abnormal function of VNIC.

Table III Experiment scenarios

Case No.		Shunt Circuit Parameters			Equivalent Mech. Parameters		
		R_t (Ω)	L (H)	C (F)	c_d (Ns/m)	m_d (kg)	k_d (N/m)
<u>Case I</u> EMSD-VFD	1.1	$+\infty$			0		
	1.2	3.8			14.7		
	1.3	1.3*			43.0		
<u>Case II</u> EMSD-VED	2.1	0.5*	0.032		111.7		1746
	2.2	0.5*	0.02		111.7		2793
	2.3	14	0.02		3.99		2793
<u>Case III</u>	3.1	1*		0.03	55.9	1.7	

EMSD-	3.2	1*		0.02	55.9	1.1	
ID	3.3	1*		0.0033	55.9	0.2	
	3.4	5.8		0.03	9.6	1.7	
Case IV	4.1	0.95*	0.034	0.0244	58.8	1.4	1643
EMSD-TID	4.2	0.5*	0.03	0.03	111.7	1.7	1862

* $R_t < R_0$ indicates the use of VNIC (i.e., $R_t = R_0 - |R_{VNIC}|$).

5.1. Case I: EMSD-VFD

As shown in Table III, Case I include three sub-cases with different total resistance R_t, which correspond to different equivalent viscous damping coefficients c_d. Fig. 6 provides the theoretical and experimental transmissibility curves of the EMSD-VFD isolator in Cases 1.1 – 1.3 in logarithm scale, where the theoretical curves are plotted based on Eq. (18). Satisfactory match is confirmed between the theoretical and experimental results. In particular, the invariant points ($\sqrt{2}, 1$) could be clearly identified. Cases 1.1 – 1.3 corresponds to different total circuit resistance values. The details are as follow:

(a) Case 1.1 corresponds to an open-circuit scenario (i.e., the equivalent resistance is infinite). Consequently, EMSD only contributes the parasitic damping force (purely mechanical damping). In this case, the peak transmissibility curve amplitude reaches $|\mathrm{H}| = 10.6$ at the resonant frequency.

(b) Case 1.2 depicts the scenario where two EM motor terminals are directly shorted, making the total circuit resistance equals to the motor inner resistance ($R_t = R_0 = 3.8$ Ω). Without the facilitation of VNIC, this scenario represents the theoretical lower limit of R_t and upper limit of the achievable equivalent damping coefficient of EMSD-VFD. The corresponding peak amplitude is $|\mathrm{H}| = 4.52$.

(c) When VNIC is introduced into the system, an equivalent negative resistance of R_{VNIC} = –2.5 Ω was generated, which reduces the total resistance to $R_t = 1.3\ \Omega$, (equivalent to an viscous damping coefficient of 47 Ns/m). The peak curve amplitude is subsequently reduced to $|\mathrm{H}| = 2$, representing a 56% decrease in comparison with Case 1.2.

In general, the resonant peak magnitude is reduced with a decrease in total circuit resistance R_t (i.e., an increase in equivalent viscous damping). The maximum achievable equivalent damping coefficient of the traditional EMSD-VFD system used to be capped by K_{em}^2 / R_0 (corresponding to Case 1.2). The introduction of VNIC proposed in this study eliminates such a limitation and increases the achievable damping value considerably. Theoretically, when the R_t value is canceled to be close to zero, the equivalent damping coefficient approaches infinity. Nonetheless, over-cancellation may cause an abnormal function of VNIC. Thus, an appropriate value should be carefully selected in real applications.

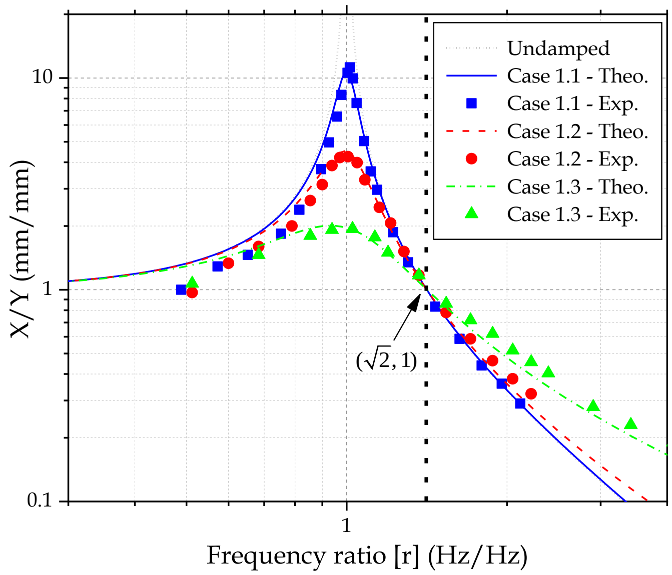

Fig. 6 Transmissibility curves of EMSD-VFD isolation with varying resistance values realized by VNIC

5.2. Case II: EMSD-VED

As shown in Table III, Case II includes two sub-cases (Cases 2.1 and 2.2) with the use of VNIC and one sub-case (Case 2.3) without the use of VNIC. Consequently, the corresponding total resistance values R_t are significantly different. Cases 2.1 and 2.2 with different L values aim to reflect the effect of the inductance on the isolation performance. Fig. 7 shows the transmissibility curves of the SDOF system with EMSD-VED, where the theoretical curves are plotted based on Eq. (20).

Fig. 7(a) compares Cases 2.1 and 2.2 that correspond to the inductance values of 0.032 and 0.02 H, respectively. According to Eq. (2), the two inductance values mimic mechanical stiffness values of 1,746 and 2,793 N/m, respectively, and represent an additional 62% and 93% stiffnesses increase to the SDOF structure relative to the original stiffness of k_h = 3,000 N/m. Such additional equivalent stiffness will increase the resonant frequency of the SDOF structure (i.e., the resonant peak shifted to right) by 27% and 39%, respectively. This frequency shifting achieved by EMSD-VED serves as an effective way to avoid excessive resonance vibration when the seismic frequency coincides with the resonant frequency of the SDOF system.

The excellent match between the theoretical and experimental curves validates the functionality of EMSD-VED. Notably, the use of the physical inductors shown in Fig. 5(c) added resistance to the circuit. Consequently, a larger R_{VNIC} is required to cancel the combined resistances of both the EM motor and the inductor to an adequately small value of $R_t = 0.5\ \Omega$ (i.e., Cases 2.1 and 2.2).

Fig. 7(b) further compares the theoretical and experimental results of Cases 2.2 and 2.3, both of which have the same inductance value of 0.02 H. However, Case 2.3 does not use VNIC module to cancel the total circuit resistance (R_t). Consequently, $R_t = 14\ \Omega$ (including inner resistances from both EM motor and inductors) in Case 2.3 is considerably larger than in Case 2.2. The discrepancy between the two curves indicates the vital role of VNIC in the successful emulation of VED.

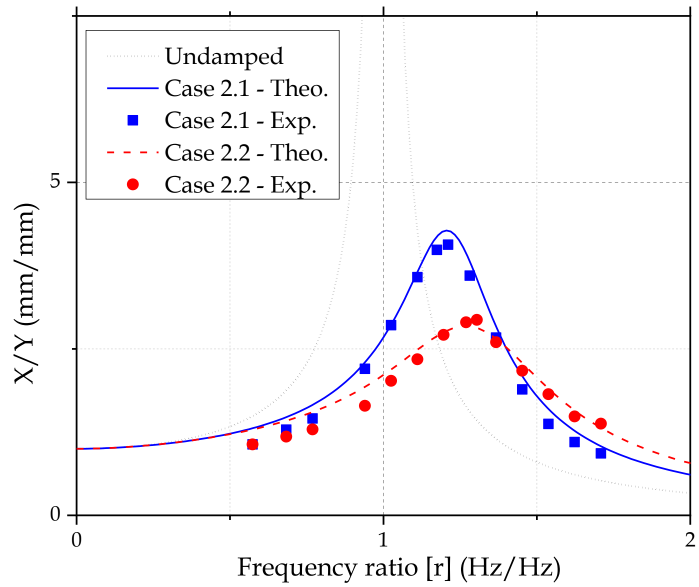

(a)

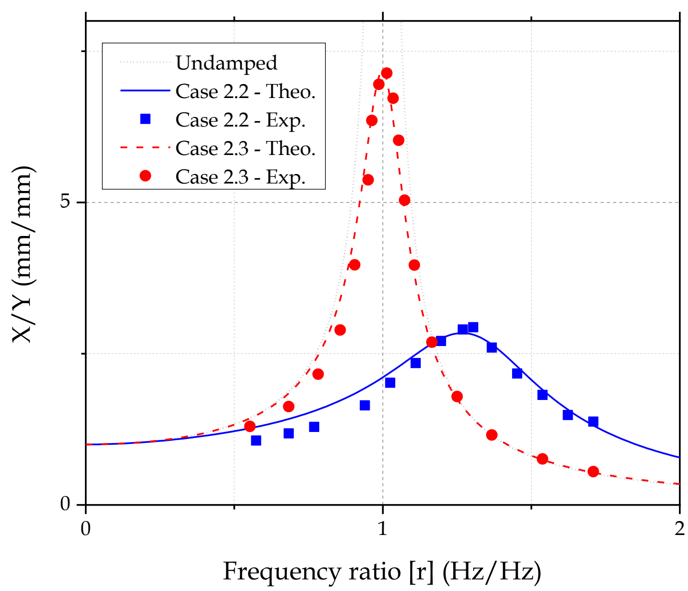

(b)

Fig. 7 EMSD-VED with various inducntance values (a) vital lines of transmissibility of EMSD-VED (b) Comparison between cases w/ and w/o VNIC

5.3. Case III: EMSD-ID

As shown in Table III, Case III includes three sub-cases (Cases 3.1 – 3.3) with the use of VNIC and one sub-case (Case 3.3) without the use of VNIC. Consequently, the former total resistance R_t is significantly smaller than the latter. In addition, Cases 3.1 to 3.3 using different C values aim to reflect the effect of the capacitance on the isolation performance. Fig. 8 compares the theoretical and experimental transmissibility curves of the EMSD-ID isolator, where the theoretical curves are based on Eq. (23). Cases 3.1 – 3.3 involved the capacitance values of 0.03, 0.02, and 0.0033 F, respectively, and the use of VNIC. According to Eq. (2), the capacitance values of 0.03, 0.02, and 0.0033 F are equivalent to virtual inertances of 1.68, 1.1, and 0.18 kg, respectively, which corresponds to mass ratios (μ) of 0.82, 0.5 and 0.08, respectively. In contrast to the situation in EMSD-VED, the increase in capacitance (i.e., equivalent inertance values) in EMSD-ID shifts the resonant frequency of the SDOF structure leftwards; the resonant frequencies decrease from 5.88 Hz to 4.47, 4.75 and 5.56 Hz (i.e., the frequency ratio is 0.76, 0.81 and 0.945) corresponding to Cases 3.1 – 3.3, respectively. Meanwhile, a lower peak profile at resonance can be observed indicating an improved isolation performance with the increase of capacitance.

Another notable feature of adopting EMSD-ID for isolation is the unfavorable vibration amplification in high frequency range (i.e., tail-up effect) in comparison to EMSD-VFD or EMSD-VED, as shown by both experimental and theoretical results in Fig. 8. A detailed explanation was provided by Hu, Chen, Shu and Huang [30].

The theoretical and experimental results of Case 3.3 (green color) do not match well in high-frequency range ($r > 2$). A possible reason is the nonlinearity of parasitic damping. As suggested by Eq. (13), the equivalent parasitic damping will increase if either the vibration amplitude or frequency is reduced (both in the denominator). In high frequency range, although the input frequency has been proportionally increased, the vibration amplitude decreases more resulting in an overall increase in parasitic damping. For instance, the comparison of responses at 5.88 Hz (i.e., system resonant frequency) and 18 Hz reveals that even though the frequency is approximately tripled, the displacement amplitude decreases more than five times as evidenced by the readings from laser displacement sensors. This condition will result in an overall increase in parasitic damping with increasing input frequency. Further provided the tail-up effect is sensitive to damping, the discrepancy between theoretical and experimental results are observed from Fig. 8(a).

Fig. 8(b) emphasizes the contribution of VNIC in the EMSD-ID isolator. The capacitance values in Cases 3.1 and 3.4 are the same and equal to 0.03 H. The only difference between the two owes to the total circuit resistance, given $R_t = 5.8\ \Omega$ in Case 3.4, which is mainly due to motor inner resistance and resistance from connection wires, whereas $R_t = 1\ \Omega$ in Case 3.1 with the facilitation of VNIC. The results of Case 3.4 exhibit neither resonant frequency shift nor amplitude reduction in comparison to Case 3.1. Hence it is concluded the capacitance effect is deterred by the large circuit resistance, which foregrounds the important function of VNIC in the proposed EMSD-ID isolator.

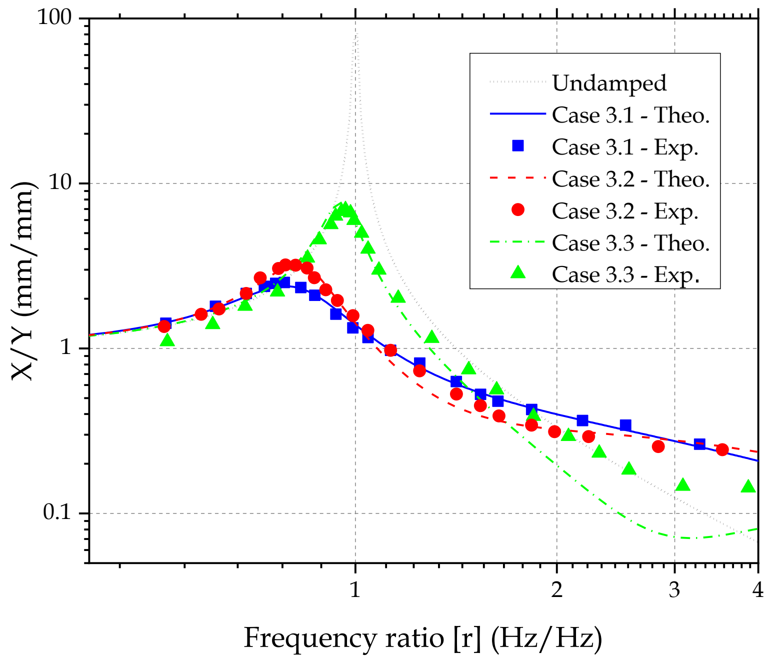

(a)

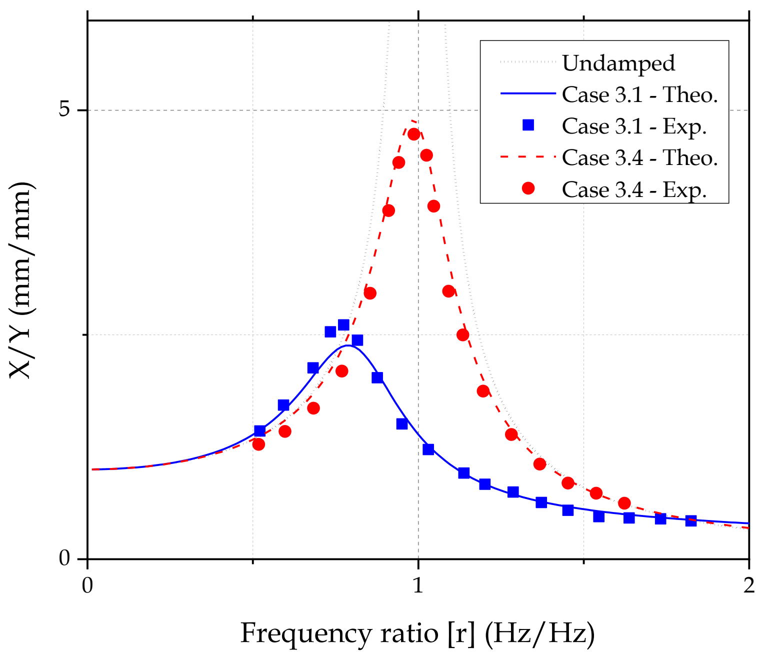

(b)

Fig. 8 EMSD-ID with various capacitance values: (a) vital lines of transmissibility of EMSD-ID, and (b) comparison of cases w/ and w/o VNIC

5.4. Case IV: EMSD-TID

EMSD-TID connects the EM motor to a series *RLC* circuit, which essentially introduces an additional degree of freedom to the structural system. The optimal parameters EMSD-TID are calculated from Eqs. (31) - (33). For instance, in the design of Case 4.1, the equivalent mass ratio (μ) is set to 0.6 to ensure an adequate control effect. The corresponding optimal capacitance is determined as C_{opt} = 0.0236 F by substituting K_{em} = 7.474 N/A and m_h = 2.2 kg into Eq. (31). Further substitution of k_h = 3000 N/m into Eq. (32) yields the optimal inductance value (L_{opt} = 0.031 H). Given that the calculation of optimal resistance (R_{opt}) requires the ζ_{opt} value, the mass ratio ($\mu = 0.6$) is used to derive ζ_{opt} using Eqs. (29) and (30), resulting in $\zeta_{opt} = 0.32$. By substituting ζ_{opt} back into Eq. (33), R_{opt} is calculated as 1.073 Ω.

A set of values (C = 0.024 F, L = 0.034 H, and R = 0.95 Ω) close to the optimal ones is adopted in Case 4.1, and the corresponding transmissibility curve is shown in Fig. 9. For a comparison purpose, another non-optimal set of parameters (C = 0.03F, L = 0.03 H, and R = 0.5 Ω) that slightly deviated from the optimal parameters is included as Case 4.2 in Fig. 9.

Fig. 9 compares the theoretical and experimental transmissibility curves of the EMSD-TID isolator, where the theoretical results are plotted based on Eq. (26). In general, a good match is observed between the theoretical and experimental results in Fig. 9, thereby validating the accuracy of both results. Cases 4.1 and 4.2 exhibit two apparent peaks in the transmissibility curves, indicating that the EMSD-TID converts the SDOF structure into an equivalent 2DOF system. Case 4.1 with the optimal parameters shows two peaks with similar heights and exhibits relatively flat shape between two peaks. Case 4.2 with the non-optimal parameters has two higher peaks with different heights and exhibits a sharper concaved shape between two peaks.

In particular, Fig. 9 includes EMSD-VFD Case 1.3 for comparison. The overall isolation performances of Cases 1.3 and 4.1 are similar in terms of peak amplitudes However, noticeable differences are observed in the parallel comparison. The EMSD-TID isolation in Case 4.1 has lower amplitude in the original resonant region ($0.7 < r < 1.1$). Moreover, EMSD-TID in Case 4.1mitigates the negative effect of high damping of EMSD-VFD in the high-frequency region ($r > 2.4$).

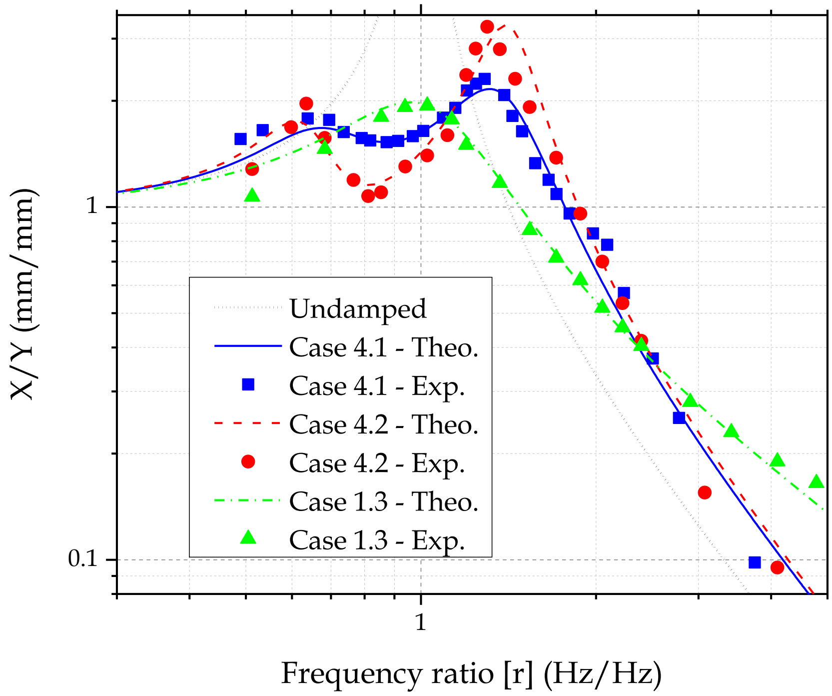

Fig. 9 Comparison between EMSD-TID and EMSD-VFD (log-log scale)

5.5. Comparison and Discussion:

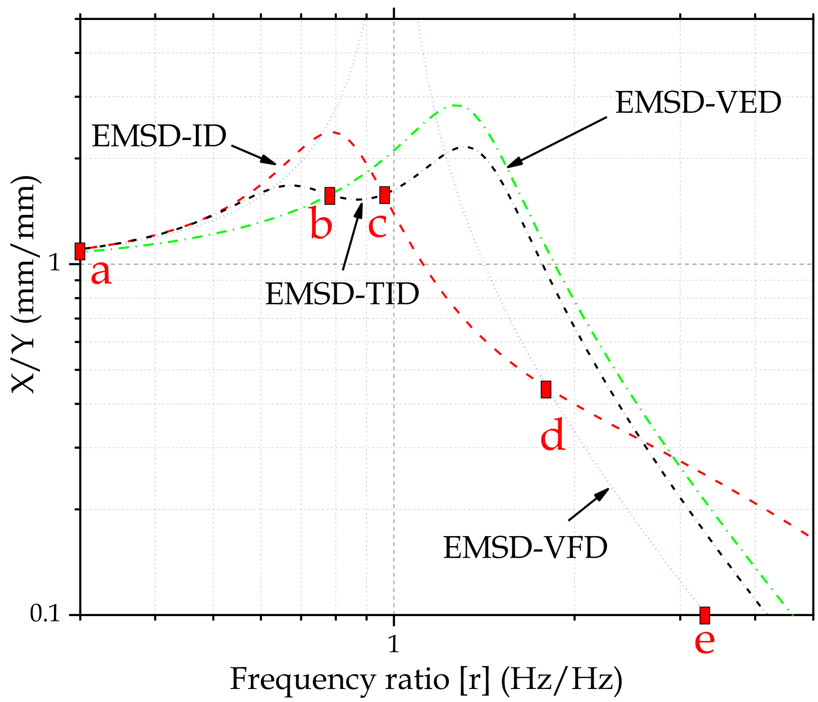

Fig. 10 Transmissibility curves of EMSDs with key points marked

Four representative conventional isolation systems are successfully emulated using the proposed EMSD-VNIC. Different versions of the EMSD isolators possess individual characteristics with regard to transmissibility curves. A representative case from each type of EMSD isolator was selected for comparison, namely, Case 1.1 (EMSD-VFD), Case 2.1 (EMSD-VED), Case 3.1 (EMSD-ID), and Case 4.1 (EMSD-TID). Fig. 10 compares their theoretical transmissibility curves; and five characteristic points (i.e., intersection points of two curves) are identified on the lowest profile of all curves, marked as points a – e. The lowest profile segment between every two adjacent points corresponds to the local optimal achievable isolation performance. The comparisons yielded the following findings about the different types of EMSD isolators.

- For frequency ratio $r \in (\mathrm{a}\,,\,\mathrm{b})$ that corresponds to a low-frequency range, EMSD-VED possesses the lowest profile, because EMSD-VED shifts the resonant frequency to the right (i.e., increases the natural frequency) by introducing extra equivalent stiffness to the system. By contrast, EMSD-ID possesses the highest profile, because it shifts the resonant frequency leftward to be closer to the excitation frequency range by introducing extra equivalent inertance to the system.
- When $r \in (\mathrm{b}\,,\,\mathrm{c})$, EMSD-TID has the lowest profile. EMSD-TID essentially introduces a second degree of freedom to the system and makes the transmissibility curve show two peaks. Consequently, the transmissibility curve

presents a saddle shape between two peaks and exhibits the best isolation performance near the original resonant region among all the cases.

- EMSD-ID has the lowest profile within range $r \in (\mathrm{c}\ ,\ \mathrm{d})$. EMSD-ID shifts the resonant peak leftward by adding equivalent inertance to the system. Besides, the transmissibility curve of EMSD-ID has a slightly concave shape between points c and d given the tail-up effect. By contrast, EMSD-VED has the highest profile in this range.

- EMSD-VFD with a low damping coefficient (e.g., Case 1.1) has the lowest profile between points d and e, revealing the well-known negative effect of high damping on isolation performance in the high-frequency range. EMSD-ID possesses the highest profile due to the "bounce back" of its tail in the high-frequency range. This result is consistent with the conclusion in the literature [30] that mechanical inerter-based isolators demonstrate poor isolation performance at high-frequency ranges. In comparison to EMSD-ID, EMSD-TID can mitigate this negative impact and improve the isolation performance in high-frequency ranges.

Notably, any adjustment in the EMSD parameters to be different from those selected in the experiment will change the transmissibility curves (i.e., the performance of each type of EMSD isolators) accordingly. Nevertheless, the comparison in Fig. 10 can still provide a qualitative understanding of the relative performance of various EMSD isolator types within different frequency ranges.

Moreover, conventional mechanical dampers normally will incorporate only one configuration; and designing a network of mechanical dampers enabling flexible switching among them would be technically difficult, if not impossible. By contrast, the proposed EMSD-VNIC isolator has a great potential to achieve this objective. Given the compact size of electrical elements, different types of shunt circuits and VNIC can be efficiently integrated into one circuit board, thus allowing for convenient switching among different circuits. Consequently, a single EMSD can demonstrate versatile mechanical behavior and thus achieve optimal isolation performance in different frequency ranges. This adaptive strategy can effectively eliminate resonant behavior when the isolated structure is subjected to sine sweeping ground excitations. The realization of such broadband isolation using EMSD warrants further studies in the future.

6. Conclusions

This paper proposes and investigates an advanced vibration isolation technique using a novel EMSD with tunable behaviors. Given conventional mechanical dampers can be emulated by EMSD by altering its shunt circuit only, four representative mechanical damper types namely, VFD, VED, ID, and TID are successfully mimicked by the proposed EMSD-VNIC system in this paper. In particular, base isolation performance of the four EMSD types (i.e., EMSD-VFD, EMSD-VED, EMSD-ID, and EMSD-TID) is studied both analytically and experimentally. The proposed EMSD with tunable behaviors intrinsically avoids stability concern compared with active control, given the emulated passive dampers allows for only one-way energy flow (i.e., from structure to EMSD). Four types of EMSDs possess complementary isolation performance within the frequency domain, i.e., each of them demonstrates the best isolation performances within an individual frequency range. These results will inspire the future development of a broadband vibration isolator by instantly switching among multiple circuits integrated in a single printed circuit board. It should also be pointed out the proposed EMSD requires energy input to the VNIC module. Nevertheless, considering the advantages over their mechanical counterparts, EMSD will be a competitive alternative in the future base isolation techniques.

Acknowledgement

The authors are grateful for the financial supports from the Research Grants Council of Hong Kong (Nos.: 15214620, PolyU 152246/18E, PolyU R5020-18, and T22-502/18-R) and the Postdoc Matching Fund Scheme from The Hong Kong Polytechnic University (W15R). The findings and opinions expressed in this paper are from the authors alone and are not necessarily the views of the sponsors.

References:

[1] Soong T T 1988 State-of-the-art review: Active structural control in civil engineering *Engineering Structures* **10** 74-84

[2] Datta T 2003 A state-of-the-art review on active control of structures *ISET Journal of earthquake technology* **40** 1-17

[3] Karnopp D 1995 Active and semi-active vibration isolation. In: *Current Advances in Mechanical Design and Production VI*, (Cairo pp 409-23

[4] Symans M D and Constantinou M C 1999 Semi-active control systems for seismic protection of structures: a state-of-the-art review *Engineering Structures* **21** 469-87

[5] Jalili N 2002 A Comparative Study and Analysis of Semi-Active Vibration-Control Systems *J. Vib. Acoust.* **124** 593-605

[6] Buckle I G 2000 Passive control of structures for seismic loads *Bulletin of the New Zealand Society for Earthquake Engineering* **33** 209-21

[7] Parulekar Y and Reddy G 2009 Passive response control systems for seismic response reduction: A state-of-the-art review *International Journal of Structural Stability and Dynamics* **9** 151-77

[8] Housner G W, Bergman L A, Caughey T K, Chassiakos A G, Claus R O, Masri S F, Skelton R E, Soong T T, Spencer B F and Yao J T P 1997 Structural Control: Past, Present, and Future *Journal of Engineering Mechanics* **123** 897-971

[9] Firestone F A 1933 A New Analogy between Mechanical and Electrical Systems *The Journal of the Acoustical Society of America* **4** 249-67

[10] Smith M C 2002 Synthesis of mechanical networks: the inerter *IEEE Transactions on Automatic Control* **47** 1648-62

[11] Makris N 1998 Viscous heating of fluid dampers. I: Small-amplitude motions *Journal of engineering mechanics* **124** 1210-6

[12] Cassidy I L, Scruggs J T, Behrens S and Gavin H P 2011 Design and experimental characterization of an electromagnetic transducer for large-scale vibratory energy harvesting applications *Journal of Intelligent Material Systems and Structures* **22** 2009-24

[13] Shen W, Zhu S and Zhu H 2016 Experimental study on using electromagnetic devices on bridge stay cables for simultaneous energy harvesting and vibration damping *Smart Mater. Struct.* **25** 1-17

[14] Zuo L and Cui W 2013 Dual-Functional Energy-Harvesting and Vibration Control: Electromagnetic Resonant Shunt Series Tuned Mass Dampers *J. Vib. Acoust.* **135** 051018-

[15] Karnopp D 1989 Permanent Magnet Linear Motors Used as Variable Mechanical Dampers for Vehicle Suspensions *Vehicle System Dynamics* **18** 187-200

[16] Graves K E, Iovenitti P G and Toncich D 2000 Electromagnetic regenerative damping in vehicle suspension systems *International Journal of Vehicle Design* **24** 182-97

[17] Gonzalez-Buelga A, Clare L R, Cammarano A, Neild S A, Burrow S G and Inman D J 2014 An optimised tuned mass damper/harvester device *Structural Control and Health Monitoring* **21** 1154-69

[18] Ding R, Wang R, Meng X and Chen L 2016 Study on coordinated control of the energy regeneration and the vibration isolation in a hybrid electromagnetic suspension *Proceedings of the Institution of Mechanical Engineers, Part D: Journal of Automobile Engineering* **231** 1530-9

[19] Marneffe B D, M. Avraam, A. Deraemaeker, M. Horodinca and A. Preumont 2009 Vibration Isolation of Precision Payloads: A Six-Axis Electromagnetic Relaxation Isolator *Journal of Guidance, Control, and Dynamics* **32** 395-401

[20] Yan B, Zhang X and Niu H 2012 Design and test of a novel isolator with negative resistance electromagnetic shunt damping *Smart Mater. Struct.* **21** 1-9

[21] Sasaki M, Kimura J and Sugiura T 2015 Vibration Suppression in High-Superconducting Levitation System Utilizing Nonlinearly Coupled Electromagnetic Shunt Damper *IEEE Transactions on Applied Superconductivity* **25** 1-5

[22] Liu Y, Lin C-C, Parker J and Zuo L 2016 Exact H2 Optimal Tuning and Experimental Verification of Energy-Harvesting Series Electromagnetic Tuned-Mass Dampers *J. Vib. Acoust.* **138** 1-12

[23] Nakamura Y, Fukukita A, Tamura K, Yamazaki I, Matsuoka T, Hiramoto K and Sunakoda K 2014 Seismic response control using electromagnetic inertial mass dampers *Earthquake Engineering & Structural Dynamics* **43** 507-27

[24] Gonzalez-Buelga A, Clare L R, Neild S A, Jiang J Z and Inman D J 2015 An electromagnetic inerter-based vibration suppression device *Smart Mater. Struct.* **24** 055015

[25] Pei Y, Liu Y and Zuo L 2018 Multi-resonant electromagnetic shunt in base isolation for vibration damping and energy harvesting *Journal of Sound and Vibration* **423** 1-17

[26] Li J-Y, Zhu S and Shen J 2019 Enhance the damping density of eddy current and electromagnetic dampers *Smart Structures and Systems* **24** 15-26

[27] Li J-Y, Zhu S, Shi X and Shen W 2020 Electromagnetic Shunt Damper for Bridge Cable Vibration Mitigation: Full-Scale Experimental Study *Journal of Structural Engineering* **146**

[28] Li J-Y and Zhu S 2018 Versatile Behaviors of Electromagnetic Shunt Damper With a Negative Impedance Converter *IEEE/ASME Transactions on Mechatronics* **23** 1415-24

[29] Zhu S, Shen W and Qian X 2013 Dynamic analogy between an electromagnetic shunt damper and a tuned mass damper *Smart Mater. Struct.* **22** 1-11

[30] Hu Y, Chen M Z Q, Shu Z and Huang L 2015 Analysis and optimisation for inerter-based isolators via fixed-point theory and algebraic solution *Journal of Sound and Vibration* **346** 17-36